An experimental study of high-velocity impact on elastic–plastic crushable polyurethane foams

CrossMark

Ali Taherkhani, Mojtaba Sadighi *, Ali Sadough Vanini, Mohsen Zarei Mahmoudabadi

Mechanical Engineering Department, Amirkabir University of Technology, Tehran, Iran

A B S T R A C T

The mechanical behavior of elastic–plastic polyurethane foams was studied experimentally under high-velocity local impact loading in normal and oblique directions, in particular, the energy absorption and the situation of damage zone were investigated. In order to obtain the mechanical properties, at first quasi-static compressive global loading was performed on the foams. Then, several samples of rigid polyurethane with different thicknesses (between 10 and 80 mm) and densities (between 40 and 320 kg/m^3) were prepared and subjected to high-velocity normal impact loading (with projectile velocity range between 30 and 140 m/s). The results showed that the foam with density of 320 (kg/m^3) at thickness of 40 (mm) has the highest energy absorption between them and also increasing the density and thickness of the foam increases the energy absorption and the area of the damage zone on rear side of the foam. Furthermore, it was found that the damage area consists of two different cylindrical and frustum-like zones. It was shown that the absorbed energy was dependent on both density and thickness; therefore, it was attempted to statistically formulize the relationship between absorbed energy on the one hand and thickness and density on the other hand based on experimental data. The effect of projectile nose including the five shapes such as flat-ended, hemi-spherical, semi-elliptical, right-conical and sharp-conical was investigated on penetration depth of projectile into the target. The results have revealed that the penetration depth increases with decreasing in the curvature radius of projectile nose cross-section; hence, the foams were too weak against sharp noses. On the other hand, performing the oblique impacts showed that increasing the oblique angle increases the damage area and changes the shape of rear side from ellipsoid-like to triangle-shape.

© 2015 Elsevier Masson SAS. All rights reserved.

1. Introduction

Properties such as cellular structure, low density, high resistance against corrosion and decay, waterproofness, absorbing harmful sunlight rays, and easy and controllable production process have made foams one of the most common cellular solids with vast applications in industry, especially in energy absorption, thermal insulation, acoustics technologies, electromagnetic wave attenuator, and also in packing industry [1].

Among the various applications of foams, utilizing them as a core in sandwich panels is increasing every day [2]. For a typical sandwich panel, face sheets are responsible for flexural rigidity, while the core provides shear load tolerance. In addition to stiffness required to keep the face sheets apart, the core must have enough shear resistance to prevent slippage relative to each other between face sheets and maintain structural continuity. Hence,

foams are one of the best materials for this purpose, which considering their cellular structure does not add much to total weight of the structure [1,2].

Bois et al. [3] categorized polymers into uncrushable elastomers, crushable foams and thermoplastic materials and studied their mechanical behavior under impact loading. They employed hyper-elasticity theory and metals plastic properties in order to study elastomers and thermoplastics, respectively. Tu et al. [4] studied plastic deformation modes of rigid polyurethane foams under static compressive loading in order to experimentally assess their mechanical behavior in raise direction of the foam as well as its lateral direction. Avalle et al. [5] studied the mechanical models of cellular solids based on stress-strain behavior. They performed the uni-axial compression tests on several types of foam (such as: EPP, PUR, EPS and PPO/PS) at different density levels and comparing the experimental results with some available models (such as: the Gibson model, the Rusch model, a modified version of Gibson model and the new empirical model). Marsavina et al. [6] investigated the role of impregnation on mechanical properties of polyurethane foams in room temperature under static and impact

* Corresponding author. Tel.: +98 21 64543448; fax: +98 21 66419736.
E-mail address: mojtaba@aut.ac.ir (M. Sadighi).

three-point bending loading, experimentally and analytically. Analysis of static loading on different types of polymeric foams and comparing its results with those of impact loading is a common subject of studies in this field [7,8].

Some of the works about the strain-rate effects have been done by researchers. Chakravarty [9] investigated the mechanical characterizations of the foams at varying strain-rates from 10^{-3} s^{-1} to 10^3 s^{-1}. He found that the compressive strength and energy absorption capacity increase with the increase in both strain-rate of loading and density of foams, but decrease with the increase in surrounding temperature. Also, Luong et al. [10] tested PVC foams at different densities under compression loading at a wide range of quasi-static and high strain-rates and obtained the same result. They understood that the mechanical properties depend on the foam density and are strain-rate sensitive; also the compressive strength and modulus increase with the foam density. The mechanical behavior of common foams (such as: EPS, HDPE and PU) has been studied at strain-rates in rang of 0.0087 to 2500 s^{-1} by Ouellet et al. [11]. In that paper, the results shown that the strain-rate effects become more pronounced at rates above approximately 1000/s; so, at above of this range the relationship between stress and strain becomes distinctly non-linear. At another work, Iannace et al. [12] investigated the linear and non-linear behavior of PP foam at a wide range of strain-rate and the correlation between strain-rate effects and viscoelastic properties of the foam was obtained using viscoelasticity theory and separating strain and time effects.

Numerical and experimental analysis of 2-D response of crushable foams under low-velocity impact loading was performed by Shim et al. [13]. They employed strikers with different cross-section geometries (cubical, cylindrical and wedge-shaped) and analyzed the effects of reducing speed of the strikers and dissipated energy on the mechanical behavior of foam. Johnson and Li [14] continued the work on effects of rigid impactor nose on penetration in other kinds of foams in order to assess the penetration resistance dependency to geometry of the impactor and density of the foam. On the other hand, Rizov [15] studied local low-velocity impact on two different densities of elastic–plastic PVC foams and analyzed their dynamic response and kinetic parameters such as contact force, load-time curve, striker speed and energy and post-impact creep response. With a more practical attitude, Yang et al. [16] assessed energy absorption capacity of polymeric foams that were used in bumpers of vehicles under different cyclic loads, including uniaxial pressure, biaxial pressure and three-point bending.

High-velocity (H-V) impact is mostly noted for scientific and research approaches especially in aerospace technology. Hedayati et al. [17] investigated the differences in bird-strike studies. They attempted to find out where the difference on pressure readings between the experimental, theoretical and numerical values come from and what the true values are. The behavior of GFRP laminates investigated by Venkatanarayanan and Stanley [18] experimentally. In their work, composite and nano-composite panels were characterized experimentally in intermediate impact response and vibration damping characteristics. Nasirzadeh and Sabet [19] attempted to assess effect of core density on ballistic resistance of sandwich panels and studied changes in the microstructures of foams. Also, Uddin et al. [20] studied experimentally the improving ballistic performance of the polyurethane foam by reinforcing with nanoparticle in projectile speed that leads to complete penetration of the target. On the other hand, Kang et al. [21] used another kind of cellular solids, honeycomb, as a core of the sandwich panel and modified the projectile diameter with considering the channeling effect in hyper-velocity impact. Improving resistance of sandwich panels with foam cores has become an interesting subject in this field; hence, Ghalami-Choobar and Sadighi [22] investigated the
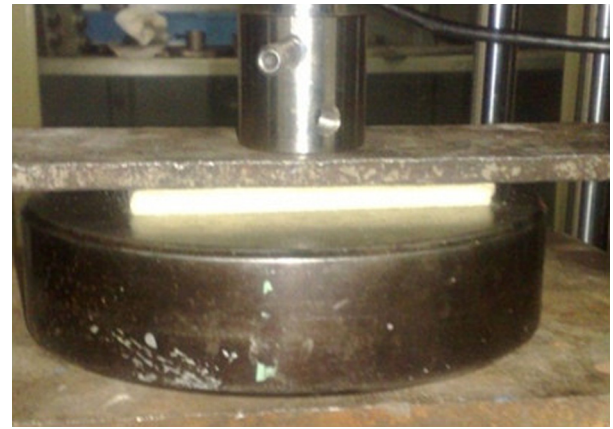

Fig. 1. Quasi-static uni-axial loading on elastic–plastic polyurethane foam.

Table 1
The results of uni-axial compression tests for utilized PU foams.

ρ (kg/m^3)	E (GPa)	σ_y (MPa)	E_{pl} (MPa)	ε_d	W (kJ)
40	3.01	0.21	0.175	0.86	29.2
80	14.61	0.96	0.63	0.79	59.5
140	39.89	2.04	2.14	0.76	148.2
180	47.63	4.22	4.63	0.73	182.9
320	114.05	6.33	8.18	0.61	340.7

H-V impact response of sandwich panels with FML face sheets and polyurethane foam core experimentally and numerically.

As discussed above, several studies were done on different types of foams under local and global conditions of quasi-static and low-velocity dynamic loadings; some of them were experimental tests while others presented numerical and analytical models. Hence, this research is dedicated to study response of crushable polyurethane foams to the H-V impact loading. In this outline, obtaining the residual velocity of the projectile leads to gain the absorbed energy in each of foam samples. Effects of the density and thickness of the foams on damage mechanisms, absorbed energy and its effective parameters are also discussed in this paper for normal and oblique impact tests. For better evaluation, the effect of projectile nose on foam's response and penetration depth studied for five of different projectile nose shapes with equal mass and same initial velocity.

2. Materials and methods

2.1. Material properties

In order to assess the energy absorption of elastic–plastic crushable polyurethane (PU) foams under H-V impact, samples with different densities were prepared and cut in various thicknesses to study the effects of the two parameters (density and thickness) on behavior of the foams. Hence, the density of 40 (kg/m^3) with thicknesses of 1, 2, 3, 4 and 8 (cm), the densities of 80 and 180 (kg/m^3) with thicknesses of 1 and 2 (cm), and the densities of 140 and 320 (kg/m^3) with thicknesses of 1, 2, 3 and 4 (cm) were prepared. Each sample is addressed with "PU X–Y" where X and Y represent thickness (in centimeter) and density (kg/m^3), respectively.

To get the better assessment of mechanical properties, the quasi-static global compression loading at speed of 5 (mm/min) by Zwick screw machine done on each sample (Fig. 1) and the stress-strain curves of the specimens plotted (Fig. 5); the results are summarized in Table 1.
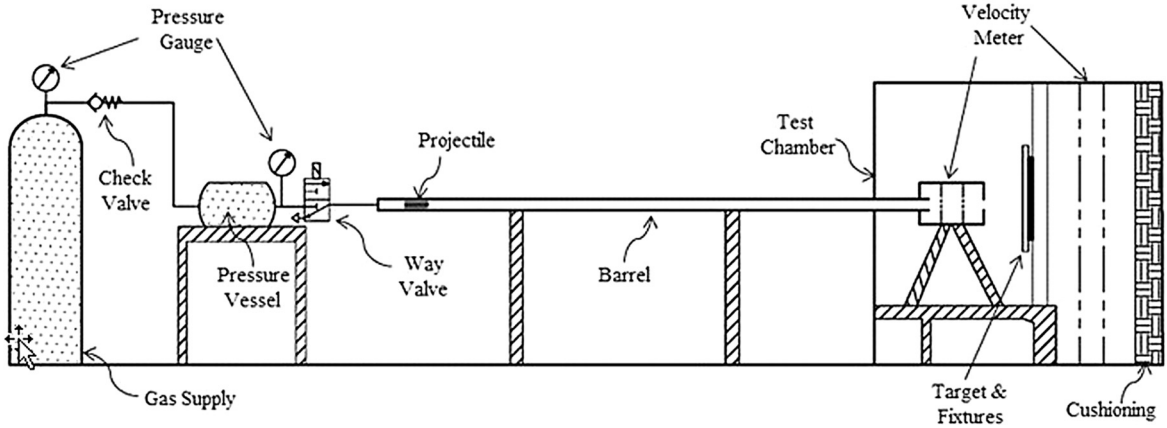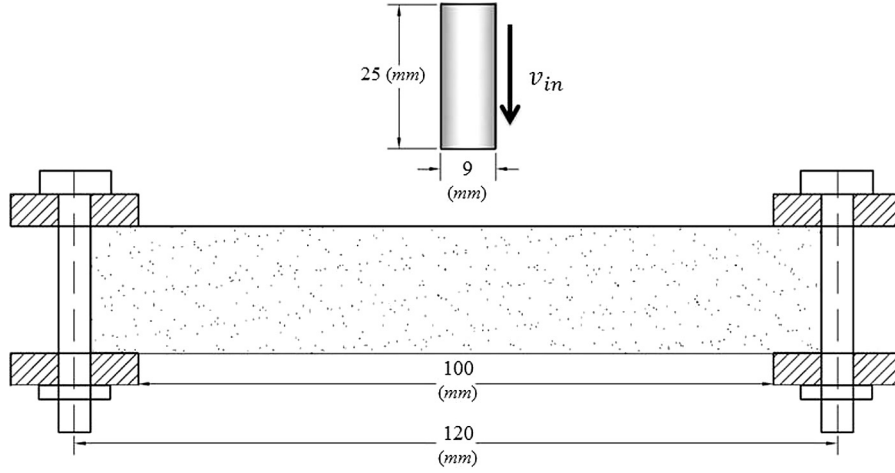
Fig. 2. Schematic of the gas gun setup.

Fig. 3. Foam sample fixed on the frame and subjected to projectile impact.

2.2. High-velocity test set-up

In H-V local impact, an object – as a projectile – is impacted into a body – as a target – at high velocity. Laboratory scale gas gun was employed in this study (Fig. 2). Pure nitrogen (99.99% purity) stored in a 40 liter gas supply under 150 bar pressure, was used in all the experimental tests. First, the required amount of gas for propelling the projectile was transferred into a smaller 4 liter pressure vessel by a check-valve. A solenoid 3/2-way valve will then open the gas path to the barrel immediately for moving the projectile in it and impacted the target. In addition to Eq. (1) which can be used in predicting speed of different projectiles (of given mass and dimensions) in terms of gas pressure and projectile moving pass into the barrel (explained in the next paragraph), an optical velocity meter (with precision of 0.1 m/s) was installed at the end of the barrel for verification of projectile speed. Another velocity meter with the same precision was installed exactly behind the frame, on which the target was fixed, in order to measure the residual speed of the projectile right after the impact. The optical velocity meter determines the velocity by measuring the time that projectile spend to pass between two optical point with the specified distance. A number of cushions were placed at the distal part of the test chamber which would trap the projectile.

By neglecting the friction and aerodynamics effects and equalizing the projectile kinetic energy with the work done on the projectile by gas, initial estimation of the projectile velocity before contact the target can be determined in terms of gas pressure and projectile placement into the barrel as below:

$$\frac{1}{2}m_p v_{in}^2 = P A_p L \xrightarrow{yields} v_{in} = \sqrt{\frac{2 P A_p}{m_p}} \tag{1}$$

in which, L is the distance that projectile passes into the barrel, P is a small vessel gas pressure, v_{in} is the initial velocities of the projectile (at the tip of the barrel; before impacted the target), m_p and A_p are the mass and the cross-section of the projectile.

Neglecting the small dissipated energy terms such as friction, the energy absorption of the target can be estimated by measuring the velocities of the projectile at the moments of entering and exiting as below [23]:

$$\frac{1}{2}m_p v_{in}^2 = E_{abs} + \frac{1}{2}m_p v_R^2 \tag{2}$$

where E_{abs} is the absorbed energy of the target and v_R is the residual velocities of the projectile. The 100×100 (mm²) squared target was fixed between two screwed plates which provided the fully-clamped condition; the dimensions of target and fixture clearly showed at Fig. 3. Furthermore, Fig. 4 implies the fixture that the screwed plate can be rotate about axis z and can provide the oblique condition. The angle of oblique can be measured by a protractor.

The impactor was a steel flat-ended projectile (SPK grade) with 12.2 (gr) mass and was propelled against the foam target with different velocities.
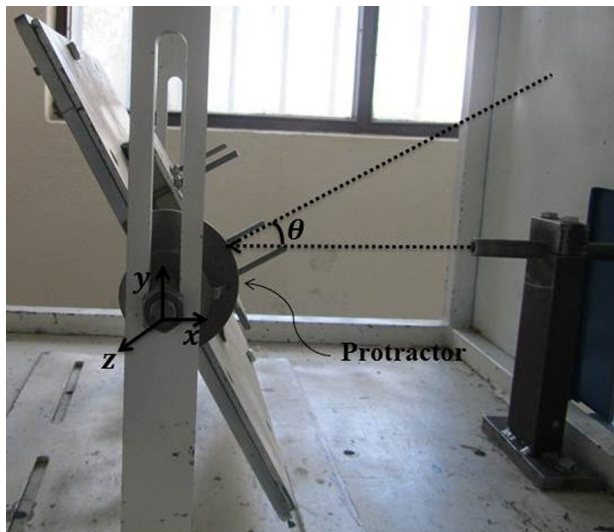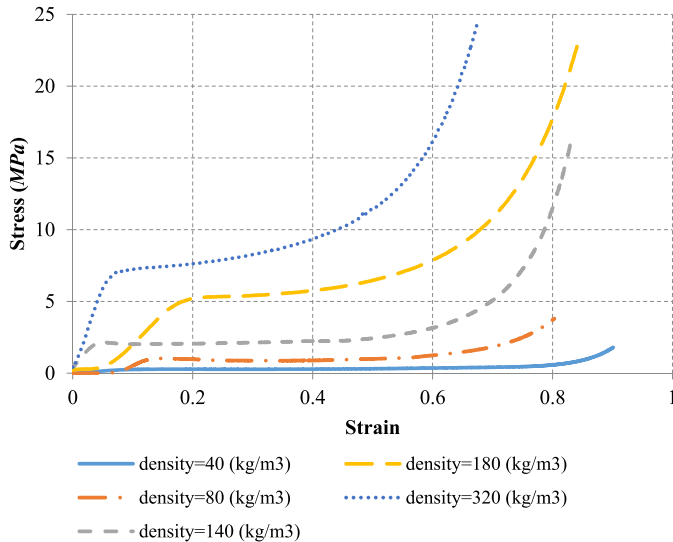
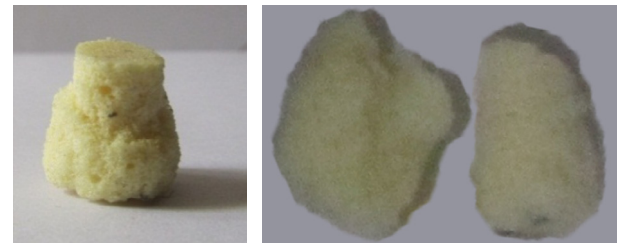**Fig. 4.** H-V oblique impact equipment.

| (a) | (b) |

Fig. 6. Shear plug (a) and fragments (b) caused by the H-V impact.

Table 2
The results of residual velocity of the projectile (in term of m/s) for some of the foam samples.

	1st test	2nd test	3rd test	4th test	5th test	6th test
PU 8-40	70.1	75.3	76.7	69.3	no data[a]	69.7
PU 3-140	90.2	87.2	83.1	85.9	87.1	—
PU 4-320	36.6	46.1[b]	39.1	37.0	35.5	38.3

[a] Unsuccessful test.
[b] Unreasonable result.

$$\lambda = \rho^{n} \qquad (3)$$

that λ is one of the mentioned parameters such as elastic modulus, E, yield stress, σ_y, the slope of plateau region, E_{pl}, the densification strain, ε_d and the absorbed energy, W and n is a real number. By substituting the data of Table 1 in the Eq. (3), the power n can be estimated as 1.7, 1.6, 1.9, −0.1 and 1.2 for E, σ_y, E_{pl}, ε_d and W respectively that are in a good agreement with the available literature.

3.2. High-velocity impact loading

Several different tests were performed to study the behavior of elastic–plastic crushable polyurethane foams under high-velocity impact and evaluating the energy absorption and its effective terms. For this reason, the effects of two parameters, foam thickness and density on the foam behavior in H-V local impact were investigated and attempted to gain the relationship between the mentioned parameters with absorbed energy as much as possible. On the other hand, the behavior of the foam in the oblique impact and the influence of the projectile nose on the penetration depth are also studied.

Various types of elastic–plastic polyurethane foams were subjected to H-V impact loading with flat nosed projectile, in order to assess energy absorption of these kinds of foams. Analysis of the tested foams revealed the effects of several terms in energy absorption mechanisms; e.g. comparing size of damage area and piercing zone of the target and considering the shear plugs and fragments demonstrate the contribution of each terms in energy absorption [24]. Close analysis of Fig. 6 shows that the striker can create fragments or/and shear plugs.

For checking the repeatability of the results, at least five H-V impact tests were done for each type of the foam samples. Then, the average of the successful and reasonable results was used to assess the residual velocity of the projectile. Those tests that yielding a data named successful test; and the reasonable result is the result that its data had difference less than 15% with the average of other's four successful tests. Table 2 provides the results of performed tests on some of the foam samples.

Table 3 presents the average results of absorbed energy (E_{abs}) and specific absorbed energy (SAE: energy absorption per unit mass) for each types of foam samples based on Eq. (2). Further, the standard deviations of the projectile residual velocities are reported in the parentheses front of v_R data. Moreover, the ballistic

Fig. 5. Stress-strain uni-axial compression curves of utilized elastic–plastic foam samples.

3. Results

3.1. Quasi-static compression loading

The stress-strain curves of the foam samples under quasi-static uni-axial compression loading have been plotted at Fig. 5. Three zones (linear-elastic, plateau and densification) are evident in these curves. In the elastic region, cell faces have only the elastic strain energy term, note the plastic hinge, while in the plateau region, plastic hinge appears. When the cells have almost completely collapsed, opposing cell walls touch and further strain compresses the solid itself, giving the final region of rapidly increasing stress and caused the densification in a foam [1]. It can be inferred from the curves that low density foams have long plateau region and experience more strain before reaching the densification region. On the other hand, it can be seen that increasing the density caused the stress-strain curve to rise.

For better comparison, the results of the uni-axial compressive tests can be listed at Table 1. According to the literature such as [1,5], the mechanical parameters of crushable foams in terms of them density, ρ, can be stated as the following relation:

Table 3
Energy absorption of different samples of elastic–plastic polyurethane foams.

Sample	v_{in} (m/s)	v_R (m/s)[a]	E_{abs} (J)	SAE (J/kg)
PU 1-40	30	28.0 (0.46)	0.70	174.5
PU 2-40	30	25.8 (0.89)	1.42	177.5
PU 3-40	64	61.1 (0.64)	2.20	183.3
PU 4-40	64	60.0 (1.03)	2.97	186.0
PU 8-40	79	72.2 (3.13)	6.30	198.2
PU 1-80	64	61.1 (0.71)	2.25	281.3
PU 2-80	64	54.2 (2.27)	7.08	442.5
PU 1-140	79	72.1 (1.96)	6.34	453.0
PU 2-140	92	77.3 (2.06)	15.20	543.0
PU 3-140	110	86.7 (2.29)	27.90	666.4
PU 4-140	110	72.8 (2.89)	41.50	741.0
PU 1-180	92	85.4 (1.22)	7.18	399.0
PU 2-180	110	93.3 (4.23)	20.71	575.2
PU 1-320	120	109.2 (3.11)	15.10	472.3
PU 2-320	120	91.8 (3.67)	36.40	568.2
PU 3-320	140	86.2 (3.33)	74.20	773.0
PU 4-320	140	37.3 (1.27)	111.08	867.8

[a] The values in the parentheses are standard deviations.

speed, v_{bal}, defined as the minimum velocity requires to projectile perforate the target completely with no meaningless residual velocity [23], are reported in Table 3. By assumption that the residual velocity in Eq. (2) is zero, value of v_{bal} can be predicted as:

$$v_{bal} = \sqrt{\frac{2E_{abs}}{m_p}} \qquad (4)$$

It must be mentioned that the efforts made in order to test all samples presented in Table 3 with the same initial velocity of the projectile were failed due to limitations of equipment and wide differences in density and thickness of the samples which led to big difference in energy absorption. For example, the ballistic speed, v_{bal}, of the foam samples PU 1-40 and PU 4-320 were about 10.8 (m/s) and 134.9 (m/s), respectively. In case of the PU 4-320 (and many other samples), the projectile with velocity of 10.8 (m/s) will strike the target without any penetration. Penetration occurs when a projectile enters a target without passing through it; while perforation occurs when a projectile pierces the target and completely passes through it [23,25]. On the other hand, if the PU 1-40 sample subjected to projectile impact with velocity of 134.9 (m/s), (considering (Eq. (2)) and energy absorption capacities listed in Table 3), it will exit from the other side with

velocity of 134.5 (m/s). It is obvious that only 0.29% difference between initial and residual velocities of the projectile is surely smaller than the tolerance of H-V impact test equipment for ballistic issue; hence performing the experimental test with the same entering velocity for all samples is not feasible (considering the current conditions).

4. Discussions

4.1. Effect of thickness in H-V impact

Based on the results presented in Table 3, energy absorption of foams changes with their thickness; i.e. it can be found a function between absorbed energy of foam and its thickness. Basically, increasing thickness of the foam, increases length of the path that the projectile passes through the foam which causes more energy dissipation. Experimental results also showed that projectile trajectory deviation from the projection direction (during the penetration) is bigger in foams with more thickness.

In order to analyze the effect of thickness, damage areas on rear sides of the samples PU X-140 and PU X-320 are illustrated in Fig. 7. It can be seen that for foams with same density, damage area increases with increasing in sample thickness. Additionally, most of damage areas, illustrated in Fig. 7, consist of a cylindrical and a frustum-like area; that is clearly visible in PU X-180 samples in Fig. 8. Attention to Figs. 7 and 8 illustrates that the frustum-like enlarges with the increasing of the foam thickness. It can be described with this fact that dominant energy terms in cylindrical area are shear and friction, while in frustum-like area, role of bending is bold.

Plotting energy absorption in terms of thickness for the results presented in Table 3 reveals an almost linear relationship between the amount of absorbed energy and thickness of the foam (Fig. 9); these linear relationships for available thickness of densities of 40, 140 and 320 (kg/m^3) were calculated and shown on each curve. The results show that the slope of the absorbed energy-thickness curve increases with density; i.e. in addition to its thickness, absorbed energy of a foam sample depends on its density also. Otherwise, it can be seen from Fig. 9 that although contributions of energy terms seem to change with thickness, but the total amount of absorbed energy changes almost linearly.
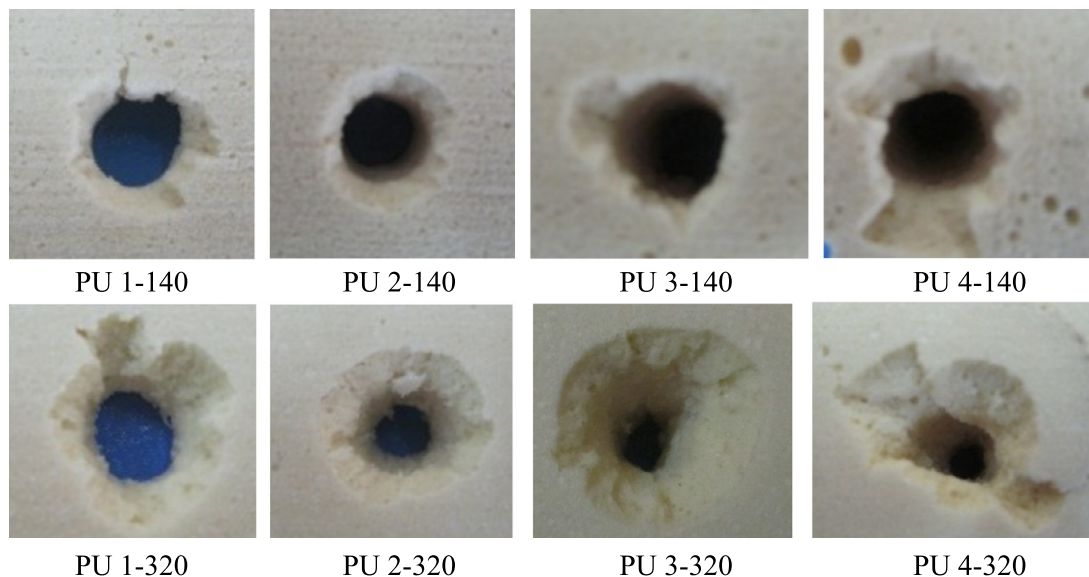

Fig. 7. Damage area on rear side of foams subjected to impact for various thickness.

Fig. 8. Sections of the PU 1-180 (top) and PU 2-180 (bottom) samples that had cylindrical and frustum-like areas.
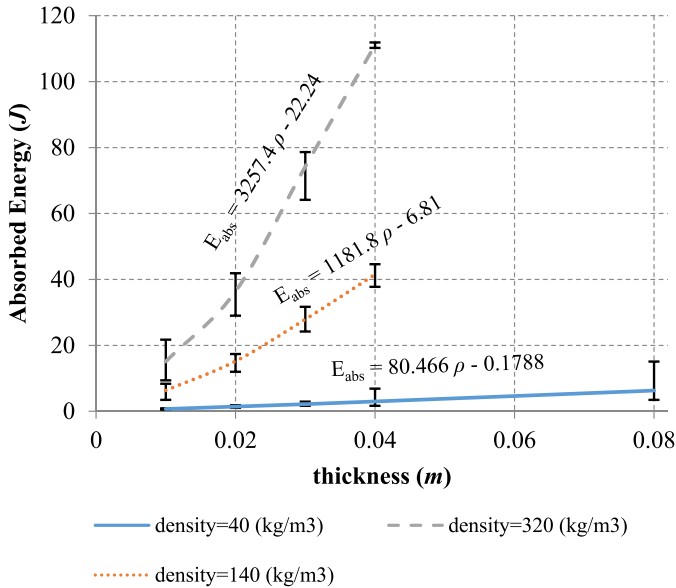

Fig. 9. Energy absorption in terms of thickness for constant densities.

4.2. Effect of density in H-V impact

Elastic-plastic polyurethane foams are materials made of a polymeric based material (e.g. polyol), a blowing agent (e.g. isocyanate) and of course various additives (for control of properties, production process and chemical reactions). During the production process, after adding the blowing agent, the polymer based material rises and becomes porous; which now can be called foam. Density of the foam depends on the extent of blowing, level of rising and the porosity. Hence, with the same polymeric base material, foams with different densities can be produced. So, mechanical properties of the foams, such as elastic modulus, stress and strain in elastic, plateau and densification zone, are strongly dependent on their density [1] (clearly explained at subsection 3.1). This is obviously seen in results of uniform quasi-static pressure tests (Fig. 5). Table 3 also shows that behavior of the foams in H-V impact depends on their density.

Fig. 10 illustrates front views of PU 4-40, PU 4-320, PU 1-80 and PU 1-180 samples after the test, which are very similar. Rear views of the PU 4-40 and PU 1-80 are closely similar to their front sides, which mean that the projectile pierced and perforated through them. On the other hand, rear side of the PU 1-180 and PU 4-320 are different with their front sides, because bending and brittle fracture terms could affect the energy absorption. Of course, increasing the density (in constant thickness) increases the damage area.

Fig. 11 illustrates damage area of rear sides of PU 2-Y samples. It can be seen that increasing the density of the foam, while thickness is constant, extends the damage area. On the other hand, length of cylinder-like area decreases while the length of the frustum-like area is increased; i.e. increasing the density leads to decreasing the shear energy contribution and increasing the bending energy (brittle fraction).

Plotting the absorbed energy values in terms of density for the results presented in Table 3 shows that there is an almost linear
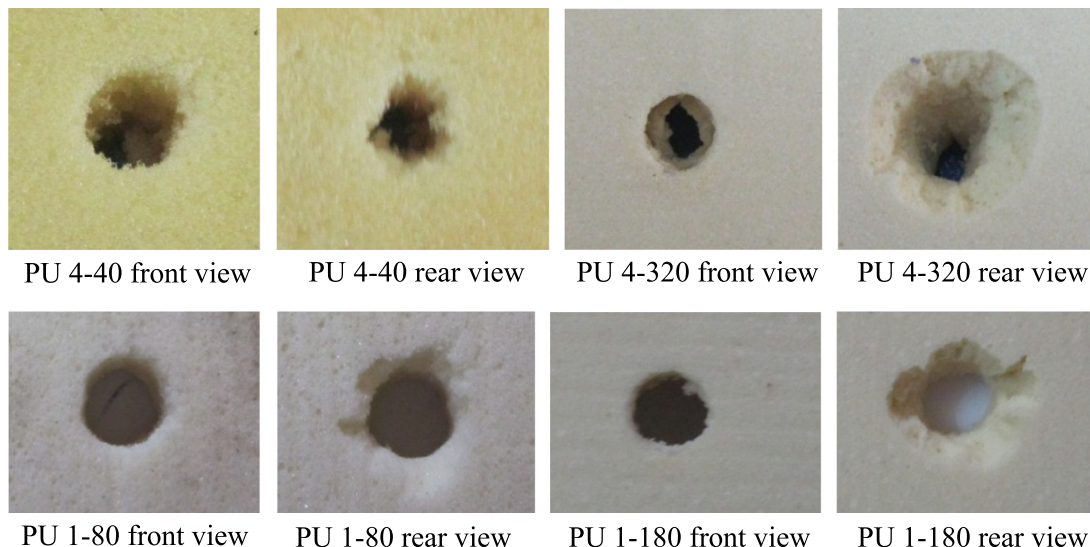

Fig. 10. Damage area on front and rear sides of elastic–plastic foams samples subjected to impact.
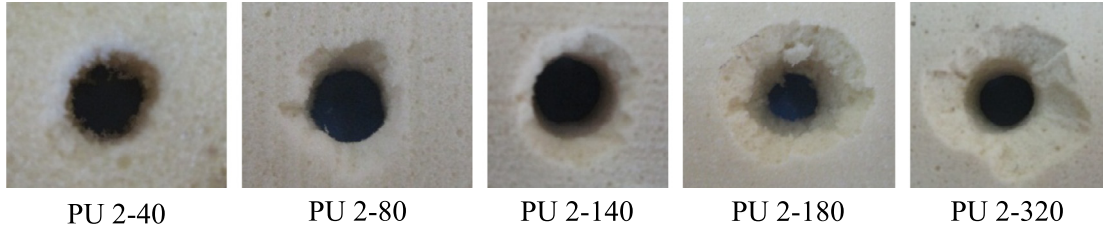
PU 2-40   PU 2-80   PU 2-140   PU 2-180   PU 2-320

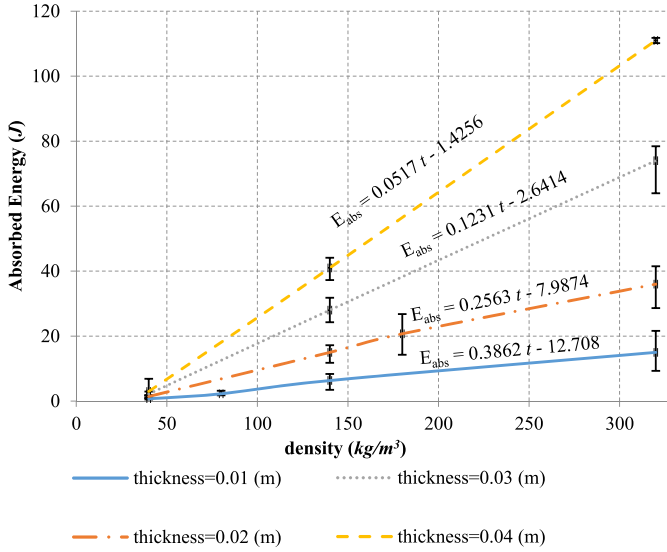**Fig. 11.** Damage area of the rear side of foams with different densities at the same thickness.

Fig. 12. Absorbed energy in terms of density for constant thickness.

relationship between absorbed energy and density of the foams (Fig. 12). The relationships have been calculated for thickness values of 1, 2, 3 and 4 (cm) of available densities. The results reveal that the slope of the linear relationship increases with thickness. This means that absorbed energy of a foam sample depends on both its density and thickness.

4.3. Statistical equation from experimental data for absorbed energy

Based on subjects expressed in previous sections, 17 samples of elastic–plastic polyurethane foams with different values of density and thickness were tested under H-V impact (Table 3). As can be seen in Fig. 9, the relationship between absorbed energy and thickness can be approximated by a linear equation (the approximation and the equation are presented in plots of Fig. 9) as:

$$E_1 = a_1 t + b_1 \qquad (5)$$

where t is thickness of the foam, E_1 is predicted energy absorption, and a_1 and b_1 are slope and intercept of plots of Fig. 9, respectively. Both a_1 and b_1 must be a function of density. In this regard, a_1 and b_1 are plotted in terms of density in Fig. 13.

Based on curves of Fig. 13, a_1 and b_1 may also be expressed in a linear approximation of density (this approximation and the obtained equations are presented in plots of Fig. 13) as:

$$a_1 = c_1 \rho + d_1 \qquad (6a)$$
$$b_1 = e_1 \rho + f_1 \qquad (6b)$$

where ρ is density of the foam, c_1 and d_1 are slope and intercept of the a_1-density curve, respectively; also, e_1 and f_1 are slope and intercept of the b_1-density curve, respectively. Replacing Eqs. (6) in Eq. (5) gives:
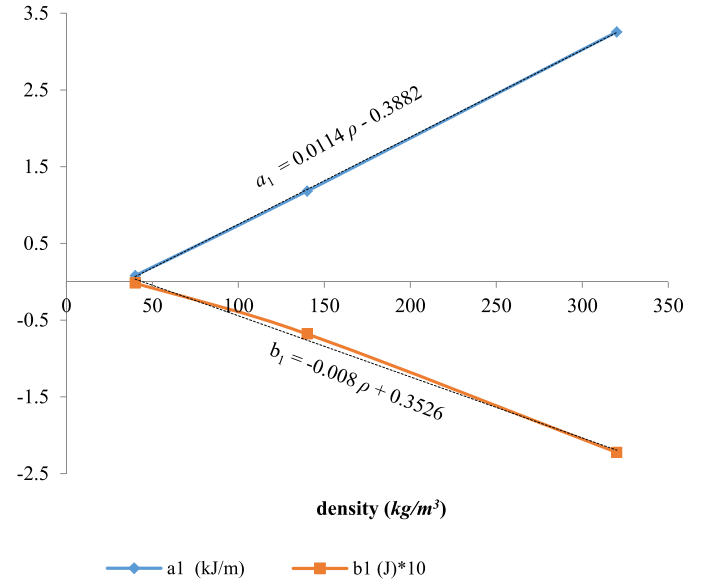

Fig. 13. Values of a_1 and b_1 in terms of density (solid line), and linear approximation (dashed line) for different values of thickness and approximated equations.

$$E_1 = c_1(\rho t) + d_1(t) + e_1(\rho) + f_1 \qquad (7)$$

where c_1, d_1, e_1 and f_1 are extracted from curves of Fig. 13 and their resulting linear approximations. Hence in SI system:

$$E_1 = 11.368(\rho t) - 388.15(t) - 0.0796(\rho) + 3.5265 \qquad (8)$$

In order to verify this equation, absorbed energy curves in terms of density can be determined for a constant thickness; these curves are plotted in Fig. 12. As the same method for assessing to E_1, it can be inferred from plots of Fig. 12 that the absorbed energy can be estimated as below:

$$E_2 = 11.266(\rho t) - 387(t) - 0.0757(\rho) + 3.3258 \qquad (9)$$

Comparing the obtained equations for absorbed energy in terms of thickness and density (Eqs. (8) and (9)) it is clear that the coefficients are almost equal; i.e. the difference between coefficients of ρt, t, ρ and the constant values of equations is only 0.9%, 0.3%, 4.9% and 5.7%, respectively. Root squares method can be employed to determine the best approximation among the obtained equations. For this purpose, the overall error [26] was calculated by comparing between statistical prediction equations (Eqs. (8) and (9)) and experimental results (Table 3) as below:

$$error = \sqrt{\frac{\sum_{i=1}^{k}\left(\frac{E_i^{pred} - E_i^{exp}}{E_i^{exp}}\right)^2}{k}} \qquad (10)$$

where E^{exp} is the absorbed energy from experiment (values of the E_{abs} column in Table 3), E^{pred} is the corresponding predicted energy absorption (from Eqs. (8) and (9)) and k is the number of tested samples. By replacing the corresponding values in Eq. (10)
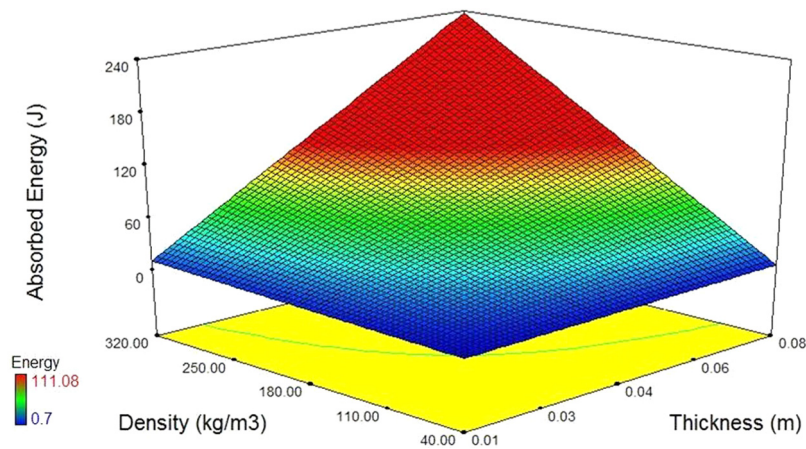
Fig. 14. The 3D graph for absorbed energy in terms of density and thickness.

$\theta = 0^{\circ}$ $\theta = 15^{\circ}$ $\theta = 35^{\circ}(a)$ $\theta = 35^{\circ}(b)$
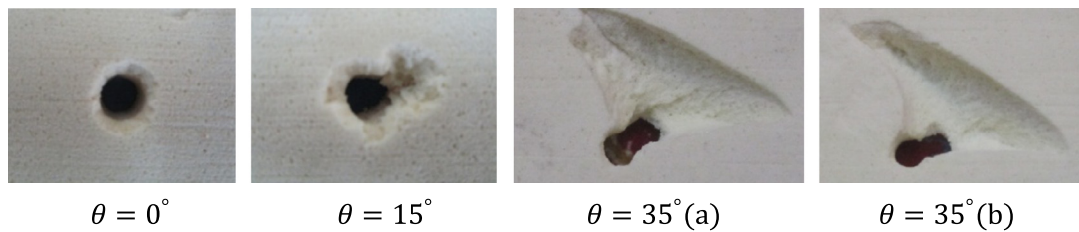
Fig. 15. Damage area on rear side of the sample impacted under different oblique tests.

can be revealed that total prediction error of Eqs. (8) and (9) with comparing by experimental results are 15.78% and 11.97%, respectively. Hence, results of Eq. (9) were the closest to the experimental values, and it yields the most accurate predictions of absorbed energy of elastic–plastic polyurethane foams with given density and thickness under H-V impacts (for the expressed conditions in section 2). The 3D curve for absorbed energy based on Eq. (9) in terms of both the density and thickness is shown in Fig. 14.

Substituting the ρ and/or t by zero gives the unrealistic results; so, it must be mentioned that the present equation is valid for densities in range 40 to 320 (kg/m^3) and thicknesses between 10 and 80 (mm) for current foams. On the other hand, it should be noted that the obtained result is a statistical equation, based on experimental data which describes the expressed situation in the best way. Performing more experimental tests with higher number of samples will of course lead to more accurate results.

In order to evaluate the obtained equation, the experimental results of PU 2-80 and PU 1-180 can be used. It must be mentioned that these two samples were excluded for obtaining the statistical equations; i.e. the approximations were performed based on the results of 15 samples other than PU 2-80 and PU 1-180. Replacing the values corresponding to these two samples in Eq. (9) and comparing between the predicted equation and experimental test data shows 6.71% and 14.92% error for PU 2-80 and PU 1-180, respectively.

4.4. Oblique test

Most experimental studies on impacts involve normal impacts. However, in real life applications, impacts are usually oblique and normal impacts are only a special case. In oblique impact, the target surface was oriented (with an oblique angle of θ) to the projection direction of the projectile. Due to the orientation of the target, the projectile has to pass through a larger thickness of the target, before exiting it. However, this would also increase target mass per surface density related to impact plane [23,27].

Table 4
The results of oblique tests.

θ (degree)	v_{in} (m/s)	v_R (m/s)[a]	E_{abs} (J)
0	92	77.3 (2.06)	15.2
15	92	75.3 (2.53)	17.1
35	92	71.9 (3.18)	20.0

[a] The values in the parentheses are standard deviations.

In order to perform the oblique test, PU 2-140 was fixed in 15° and 35° angles (Fig. 4) employing a scaled plane (protractor), and subjected in impact by 92 (m/s) velocity (properties of the projectile, dimensions of the sample and boundary conditions are according to the section 2); then, the results were compared with that of normal impact. For checking the repeatability of the results, at least five H-V impact tests were done for each type of the foam samples. Fig. 15 illustrates damage area on rear side of the foam tested under 0°, 15° and 35° oblique angles. Further, two samples of the foam tested in $\theta = 35^{\circ}$ have been shown at Fig. 15 as $\theta = 35^{\circ}$ (a) and $\theta = 35^{\circ}$ (b); so, comparison between $\theta = 35^{\circ}$ (a) and $\theta = 35^{\circ}$ (b) shows the very good repeatability. It shows that the damage area is bigger in oblique test and also its shape changes from circular into elliptical. It can be seen that at large angles, the projectile separated a piece of foam with triangular shape while piercing the foam. Base of the triangle is parallel to diameter of the initial circular hole and its apex shows direction of the exit path like an arrow.

Results of these tests are summarized in Table 4 and Fig. 16 that implied that absorbed energy increases for oblique angles smaller than $\theta = 35^{\circ}$. On the other hand, the absorbed energy in terms of projection direction curve shows that (for not very large angles) absorbed energy increases approximately linear with angle of impact.

Considering t as thickness of target in normal impact, thickness of target for oblique impact (t_{θ}) would be [27]:

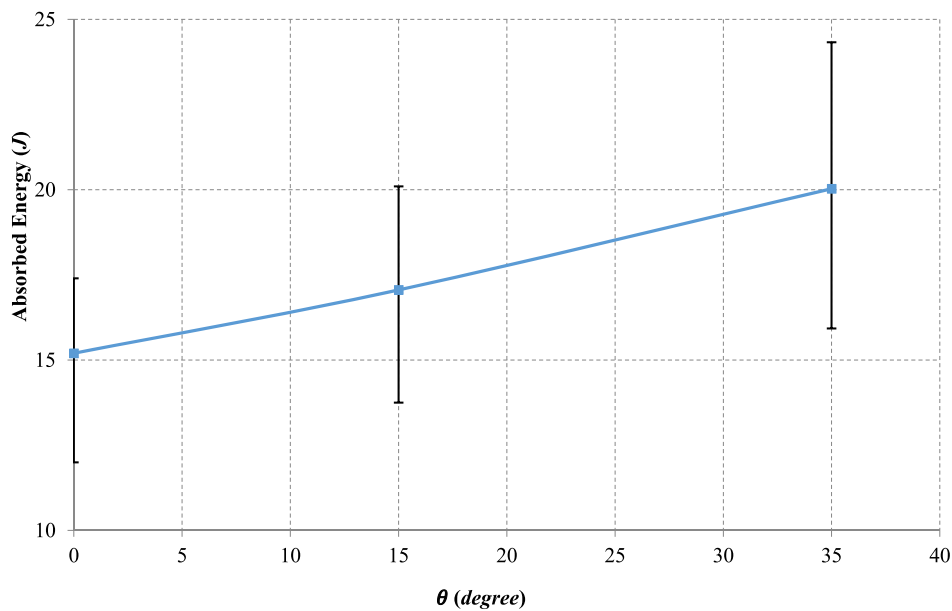$$t_{\theta} = \frac{t}{\cos\theta} \tag{11}$$

Fig. 16. Absorbed energy against with angle of contact.

Fig. 17. Penetration and embedment of projectile in crushable polyurethane foam under H-V impact.

The experimental results show that the mentioned energy absorption relationship (Eq. (9)) can be utilized for estimation the absorbed energy of the oblique tests by replacing t with t_θ. Hence, Eq. (9) (characterized by t_θ) evaluates the absorption energy with 2% and 9% difference with the obtained data from experimental test for 15° and 35°, respectively.

4.5. Effect of projectile nose on penetration depth

Geometry of the projectile nose could significantly affect quality of piercing by the penetrator in the target. Therefore, the efforts in this section were based on to assess the effect of projectile nose on the penetration. For this purpose, a foam sample with density of 140 (kg/m^3) and thickness of 6 (cm) was cut from the same block as other samples with this density. Speed of projectiles was set in a way that the projectile would only locally penetrate the target but could not perforate through it (Fig. 17).
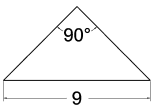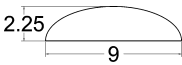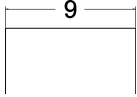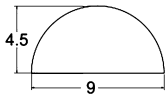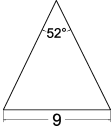
Five steel projectiles (of SPK grade) with different nose geometries, including flat-ended, semi-elliptical, hemi-spherical, right-conical with apex angle of 90° and sharp-conical with apex an-gle of 52° were prepared. Table 5 lists complete details of these projectiles. In order to be able to correctly assess the effect of projectile nose, efforts were made to prepare all projectiles with the same diameter of 9 (mm) (hence differences in damages would not be the results of different diameters), and length of their cylindrical part was chosen in a way that they had the same mass (15 (gr)). All tests were performed with the initial velocity of 33 (m/s). A digital caliper was used for measurement of penetration depth.

It can be seen from the results presented in Table 5 that changing the projectile nose from flat and make it sharper increases the penetration depth and decreases of the energy absorption capacity. In other words, foams show more crushing resistance against blunt projectiles comparing with non-flat nose shapes. Because in flat nose shape, direction of the exerted load by these projectiles is perpendicular to the target surface (equal with principal direction) and in this direction foams have the most resistance [14,24]. Since the foam cells tend to take the shape of the impactor [24], they will be pulled inward and placed in an oblique position in case of. In this situation, the force is exerted in a direction other than the rising direction of the foam; therefore the projectile can more penetrate because of the smaller strength along the direction of the force. So, penetration depth of SEP projectile, which has the closest geometry to FLT projectile, showed the smallest increase (only 15.6%). Additionally, penetration depth was increased 26.3%, 45.8% and 82.1% in case of HSP, RCN and SCN projectiles, respectively.

Differences between the SEP and FLT results is smaller than those of the HSP and FLT result; hence, its penetration depth is 8.4% less than the latter one. On the other hand, shear and tear resistance of the foam is smaller against projectiles with sharper noses. Thus comparing the results for RCN and SCN projectiles reveals that the sharper nose penetrated 24.9% deeper. It is also notable that changing geometry of the nose from HSP into sharp-ended (e.g. conical) decreases shear resistance of the target structure; of course sharp-ended projectile increases stress concentration (which causes tear or rupture) in contact zone. This fact ex-plains the 26.1% difference in penetration depth of SEP and RCN projectiles, which have the same mass and the same length of cylindrical section (hence friction affects them almost equally). Additionally, despite equal mass and equal length of cylindrical section, penetration depth of SCN projectile is 44.2% more than that of the HSP projectile.

Table 5
Effect of nose geometry of the steel projectiles on penetration depth.

Type	Right-conical	Semi-elliptical	Flat	Hemi-spherical	Sharp-conical
Projectile index	RCN	SEP	FLT	HSP	SCN
Nose geometry					
Cylindrical length (mm)	28.5	28.5	30	27	27
Global schematic					
Penetration depth (mm)[a]	26.1 (0.55)	20.7 (0.49)	17.9 (0.34)	22.6 (0.43)	32.6 (0.78)

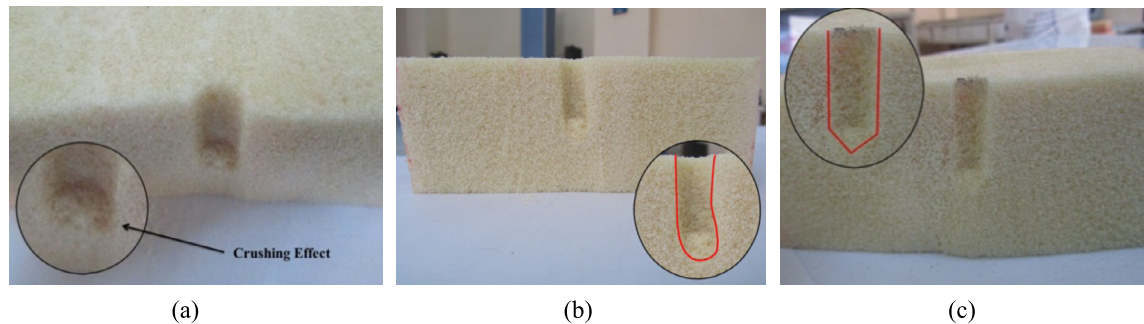[a] The values in the parentheses are standard deviations.

Fig. 18. Cross-section view of projectile penetration; (a) crushing effect, (b) HSP nose effect, and (c) conical nose effect.

Fig. 18 illustrates cross section views of some of the foams that were subjected to impact of various types of projectile noses. Investigating the results of FLT projectile shown in Fig. 18(a), reveals that crushing of the cells can be observed at the bottommost points of penetration. Actually during penetration process, the projectile crushes all material beneath itself. Thus, the crushing term may also be considered as another term of energy involved in controlling of projectile movement and dissipation of its kinetic energy. Figs. 18(b) and 18(c) also show that foam cells near the contact zone tend to take the shape of the projectile nose; these figures show shape of the projectile body inside the foam. They also show that the projectiles slightly deviated during penetration; this deviation is small in case of projectiles with sharper noses. Gravity effect, inherent anisotropy and inhomogeneity can be proposed as the reason of deviations; unfortunately most of them are rarely considered in finite element simulations.

5. Conclusion

In this study, rigid polyurethane foam samples with different densities and thicknesses were subjected to high-velocity impact loadings in both normal and oblique cases with different projectile nose shapes.

The results showed that increasing the thickness of foam increases the absorbed energy and damage area; but also increases the probability of projectile trajectory deviation into the penetration zone. Hence, the results implied that the projectile perforation path makes damage zone into two parts: a cylindrical (where dominant energy terms are shear and friction) and a frustum-like (where role of bending and brittle fracture is bold). Also, increasing foam density increases the area of the damage zone and absorbed energy of the foam, decreases the length of cylindrical part and increases the area of frustum-like part.

It was found that the damage zone has major dependence to angle of contact. In oblique impact, the damage area in low-angle impact is similar to an ellipsoid; but increasing the oblique angle changes the damage area shape to triangular-shape.

Investigation on the projectile nose effects showed that the foams have higher strength against projectile with flat nose compared to elliptical noses. Moreover, they are too weak against sharp-nosed projectiles.

In this article, based on the experimental data, a bilinear relationship was presented for estimation of the polyurethane rigid foam absorbed energy as a function of density and thickness simultaneity. In addition, the mentioned equation can be utilized for evaluating the absorbed energy in the oblique condition by replacing the normal thickness with apparent thickness.

Conflict of interest statement

None declared.

References

[1] L.J. Gibson, M.F. Ashby, Cellular Solids: Structure and Properties, second edn., Cambridge University Press, 1997.
[2] J.R. Vinson, The Behavior of Sandwich Structures of Isotropic and Composite Materials, CRC Press, 1999.

[3] P.A. Du Bois, S. Kolling, M. Koesters, T. Frank, Material behavior of polymers under impact loading, Int. J. Impact Eng. 32 (2006) 725–740.

[4] Z.H. Tu, V.P.W. Shim, C.T. Lim, Plastic deformation modes in rigid polyurethane foam under static loading, Int. J. Solids Struct. 38 (2001) 9267–9279.

[5] M. Avalle, G. Belingardi, A. Ibba, Mechanical models of cellular solids: parameters identification from experimental tests, Int. J. Impact Eng. 34 (2007) 3–27.

[6] L. Marsavina, T. Sadowski, M. Knec, R. Negru, Non-linear behavior of foams under static and impact three point bending, Int. J. Non-Linear Mech. 45 (2010) 969–975.

[7] A. Gilchrist, N.J. Mills, Impact deformation of rigid polymeric foams: experiments and fea modeling, Int. J. Impact Eng. 25 (2001) 767–786.

[8] M. Avalle, G. Belingardi, R. Montanini, Characterization of polymeric structural foams under compressive impact loading by means of energy-absorption diagram, Int. J. Impact Eng. 25 (2001) 455–472.

[9] U.K. Chakravarty, An investigation on the dynamic response of polymeric, metallic, and biomaterial foams, Compos. Struct. 92 (2010) 2339–2344.

[10] D.D. Luong, D. Pinisetty, N. Gupta, Compressive properties of closed-cell polyvinyl chloride foams at low and high strain rates: experimental investigation and critical review of state of the art, Composites, Part B, Eng. 44 (2013) 403–416.

[11] S. Ouellet, D. Cronin, M. Worswick, Compressive response of polymeric foams under quasi-static, medium and high strain rate conditions, Polym. Test. 25 (2006) 731–743.

[12] F. Iannace, S. Iannace, G. Caprino, L. Nicolais, Prediction of impact properties of polyolefin foams, Polym. Test. 20 (2001) 643–647.

[13] V.P.W. Shim, Z.H. Tu, C.T. Lim, Two-dimensional response of crushable polyurethane foam to low velocity impact, Int. J. Impact Eng. 24 (2000) 703–731.

[14] E.A. Flores-Johnson, Q.M. Li, Indentation into polymeric foams, Int. J. Solids Struct. 47 (2010) 1987–1995.

[15] V.I. Rizov, Low velocity localized impact study of cellular foams, Mater. Des. 28 (2007) 2632–2640.

[16] X. Yang, Y. Xia, Q. Zhou, Influence of stress softening on energy-absorption capability of polymeric foams, Mater. Des. 32 (2011) 1167–1176.

[17] R. Hedayati, M. Sadighi, M. Mohammadi-Aghdam, On the difference of pressure readings from the numerical, experimental and theoretical results in different bird strike studies, Aerosp. Sci. Technol. 32 (2014) 260–266.

[18] P.S. Venkatanarayanan, A.J. Stanley, Intermediate velocity bullet impact response of laminated glass fiber reinforced hybrid (HEP) resin carbon nano composite, Aerosp. Sci. Technol. 21 (2012) 75–83.

[19] R. Nasirzadeh, A.R. Sabet, Study of foam density variations in composite sandwich panels under high velocity impact loading, Int. J. Impact Eng. 63 (2014) 129–139.

[20] M.F. Uddin, H. Mahfuz, S. Zainuddin, S. Jeelani, Improving ballistic performance of polyurethane foam by nanoparticle reinforcement, J. Nanotechnol. (2009) 794740, 8 pages.

[21] P. Kang, S.K. Youn, J.H. Lim, Modification of the critical projectile diameter of honeycomb sandwich panel considering the channeling effect in hypervelocity impact, Aerosp. Sci. Technol. 29 (2013) 413–425.

[22] M. Ghalami-Choobar, M. Sadighi, Investigation of high velocity impact of cylindrical projectile on sandwich panels with fiber–metal laminates skins and polyurethane core, Aerosp. Sci. Technol. 32 (2014) 142–152.

[23] S. Abrate, Impact on Composite Structures, Cambridge University Press, 1998.

[24] M.E. Backman, W. Goldsmith, The mechanics of penetration of projectiles into targets, Int. J. Eng. Sci. 16 (1978) 1–99.

[25] M.L. Wilkins, Mechanics of penetration and perforation, Int. J. Eng. Sci. 16 (1978) 793–807.

[26] P.R. Bevington, D.K. Robinson, Data Reduction and Error Analysis for the Physical Sciences, third edn., McGraw-Hill, United States, 2003.

[27] R. Zaera, Impact engineering of composite structures, in: S. Abrate (Ed.), International Center for Mechanical Science, CISM Courses and Lectures, Udine, Italy, 2011, pp. 305–403.